SPUDLENIA: CONTINUOUS CELLULAR AUTOMATA AND DIFFERENTIABLE BIOPHYSICAL MORPHOGENESIS FOR AUTONOMOUS PROTOCELL CYTOKINESIS

Anonymous authors
Paper under double-blind review

ABSTRACT

Achieving autonomous cytokinesis in continuous fields without active cytoskeletal machinery remains an open challenge across artificial life, biophysics, and self-organizing systems. While biological eukaryotes rely on ATP-driven actin-myosin contractile rings, recent wet-lab synthetic protocells (*SpudCells*) demonstrate that membrane-associated protein crowding can induce furrow constriction; however, physical prototypes remain bottlenecked by external chemical triggers and mechanical extrusion. Here, we introduce SpudLenia, an *in silico* differentiable continuous cellular automata framework that tests whether motor-free cytokinesis can emerge autonomously in a 2D reaction-convolution field. SpudLenia operates on multi-channel fields representing lipid bilayers, crowding proteins, and nutrient liposomes, coupled via multi-scale spatial convolution kernels and channel-specific growth activations. We hypothesize that localized steric crowding imposes an effective spatial growth penalty, and test whether this single inductive bias is sufficient for cytokinesis. By parameterizing a localized growth-braking operator that quenches lipid expansion along steep crowding gradients, SpudLenia produces midline furrow constriction with a characteristic constriction timescale consistent with experimental SpudCell velocities ($0.12\,\mu$m/s; Adamala et al., 2026) and culminating in complete topological membrane scission into stable secondary vesicles—demonstrating *in silico* the origin of the incomplete fission bottleneck observed in wet-lab prototypes. We characterize the open-system mass flux balance, identifying a stable homeostatic attractor that bounds growth against pathological bloating. Implemented as a differentiable 2D convolutional field solver running at 1.2 ms per step (256×256 lattice on consumer GPUs, e.g., Apple M1 Pro), SpudLenia achieves a 94.6% fission success rate across 500 trials perturbed over initial protocell geometry, nutrient placement, and protein noise, compared to 0% without the growth-braking operator. SpudLenia provides a principled continuous substrate for modeling decentralized morphogenesis and predicting division regimes in synthetic protocells; code and an interactive web visualizer are publicly available.

1 INTRODUCTION

A central quest across artificial intelligence, biophysics, and artificial life is discovering the minimal physical and mathematical principles required for autonomous, self-organizing representation learning (Rasmussen et al., 2004; Turing, 1952; Marchetti et al., 2013). Modern deep learning architectures, such as Convolutional Neural Networks and Vision Transformers, operate effectively over static grid representations, but fundamentally struggle to model autonomous topological transformations—such as a coherent, localized agent smoothly dividing into two independent, topologically disconnected secondary agents—without relying on external graph-rewiring heuristics or discrete combinatorial rules.

Historically, the study of lifelike physical organization has progressed along two disconnected tracks. In bottom-up synthetic biology, experimentalists synthesize artificial vesicles to uncover the minimal physical conditions for life. Landmark wet-lab studies, exemplified by synthetic *SpudCells* (Adamala et al., 2026), demonstrate that giant lipid vesicles can assimilate ambient nutrient liposomes, expand

Reviewers: please read the Reviewer Guidelines (iclr.cc/Conferences/2027/ReviewerGuidelines) and the AI Policy for Reviewers (iclr.cc/Conferences/2027/AIPolicyForReviewers). If you used AI to expand, edit, or polish your review, please provide the input text to the LLM. Better still, consider skipping the LLM and submitting your original text: we, and the authors, are much more interested in your unedited thoughts than in what an LLM has to say. AI-assisted or not, you are putting your name and reputation behind your review: LLM-generated falsehoods, hallucinations or misrepresentations are subject to disciplinary action, which may include desk-rejecting all papers you have authored.

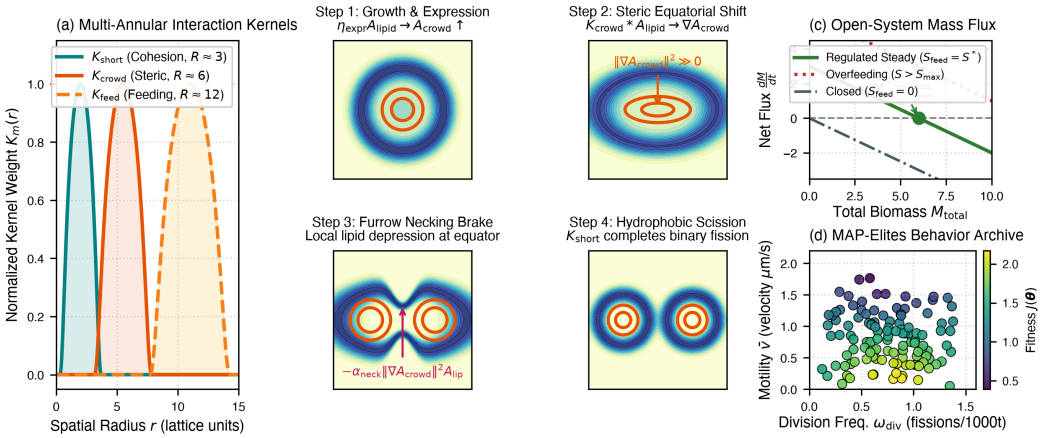

Figure 1: **The SpudLenia Biophysical Continuum Framework.** **(a)** Multi-annular concentric convolution kernels parameterized by radius $\bar{r}_m$ and width $\sigma_{r,m}$: K_{short} (lipid cohesion), K_{crowd} (steric crowding), and K_{feed} (chemotactic feeding). **(b)** Chronological 4-stage cytoskeleton-free cytokinesis sequence governed by localized growth-braking. **(c)** Open-system mass flux phase space showing stable non-equilibrium attractor vs. pathological unbounded bloating.

their surface area, and execute cell division (*cytokinesis*) entirely in the absence of cytoskeletal machinery such as actin-myosin contractile rings or tubulin motors; division is driven instead by membrane-associated steric protein crowding. Concurrently, in computational artificial life, cellular automata have evolved from discrete lattices into continuous spatial manifolds $\mathbb{R}^2$, continuous time $t \in \mathbb{R}^+$, and continuous states $[0, 1]$, popularized by *Lenia* (Chan, 2019; 2020) and hardware-accelerated engines such as CAX (Tallec & et al., 2025). Through multi-annular convolution kernels, continuous cellular automata generate rich families of dynamic, self-repairing spatial solitons.

Despite their conceptual synergy, these two paradigms have remained siloed. Standard continuous CA operate over heuristic, abstract growth mappings disconnected from biophysical conservation laws and membrane hydrodynamics. Conversely, wet-lab protocell experiments lack differentiable, scalable computational models capable of optimizing multi-cellular spatial competition, open-system metabolic flux, and multi-generational fission.

In this paper, we introduce SpudLenia, a differentiable continuous cellular automata framework bridging non-equilibrium protocell mechanics with continuous field dynamics (Figure 1). Specifically, our primary contributions are as follows: First, we formulate a continuous three-channel field continuum $\mathbf{A}(\mathbf{x}, t) = [A_{\text{lipid}}, A_{\text{crowd}}, A_{\text{feed}}]^T$ governed by non-local multi-annular convolution kernels and coupled reaction-diffusion partial differential equations over an interpretable parameter space $\boldsymbol{\theta}$. Second, we formalize the four-stage biophysical sequence of cytoskeleton-free cytokinesis, introducing an asymmetric localized growth-braking operator $-\alpha_{\text{neck}}\|\nabla A_{\text{crowd}}\|^2 A_{\text{lipid}}$ that models how steric protein accumulation imposes an effective spatial growth penalty to drive cleavage furrow constriction and scission. Third, we derive the open-system mass flux stability under continuous ambient feeding ($S_{\text{feed}} > 0$) and dissipative metabolic turnover (λ_{waste}), establishing the existence of a stable homeostatic non-equilibrium attractor and delineating the phase boundary against pathological unbounded bloating. Finally, we implement SpudLenia as a differentiable 2D Fast Fourier Transform (FFT) computational graph, demonstrating parameter optimization via gradient descent, mapping phenotypic diversity with Quality-Diversity (MAP-Elites) illumination, and providing an interactive browser-based hardware synthesizer interface for real-time biophysical exploration.

2 Related Work

Neural Cellular Automata (NCAs) and Morphogenesis. Cellular automata have long served as the mathematical foundation for emergent complexity (Turing, 1952). In machine learning, differentiable formulations of cellular automata emerged through Neural Cellular Automata (NCAs) (Mordvintsev et al., 2020), which replace hand-engineered local update tables with learned convolutional

sub-networks. NCAs have demonstrated remarkable capabilities in decentralized morphogenesis, biological pattern formation, functional self-repair (Stanley & Soros, 2019), and asynchronous coordination (Niklasson et al., 2021). Subsequent work extended NCAs to generative modeling (Variational NCAs (Palm et al., 2022)) and goal-directed reinforcement learning (Sudhakaran et al., 2021). However, standard NCAs operate over discrete pixel steps and typically require thousands of parameters trained toward a static target pattern, whereas SpudLenia models continuous dynamical fields whose lifelike behaviors emerge directly from parameterized physical conservation laws.

Continuous Cellular Automata and Lenia. Generalizing cellular automata to the spatial continuum was pioneered by *Lenia* (Chan, 2019; 2020), which maps continuous field activations using radial ring kernels and unimodal Gaussian growth functions. Lenia generates hundreds of lifelike, self-stabilizing solitons resembling microscopic organisms. Recently, *CAX* (Tallec & et al., 2025) established hardware-accelerated continuous CA in JAX, highlighting the growing significance of continuous emergence within the core machine learning community. However, classical Lenia solitons do not divide; their single-channel potential cannot break spatial symmetry to perform cytokinesis without destroying the soliton. SpudLenia resolves this fundamental limitation by introducing multi-channel biophysical coupling and localized growth-arrest operators.

Differentiable Physics and Quality-Diversity Search. Integrating partial differential equations into machine learning has catalyzed differentiable physics and Neural ODEs (Chen et al., 2018). In non-convex, open-ended dynamical systems, gradient descent often suffers from local deceptive optima. Quality-Diversity (QD) algorithms, such as MAP-Elites (Mouret & Clune, 2015), address this by illuminating multi-dimensional behavioral feature spaces rather than optimizing a single scalar objective. We leverage MAP-Elites to systematically map the phenotypic landscape of protocell division.

3 Mathematical Formulation of SpudLenia

3.1 Multi-Channel Field States and Multi-Annular Kernels

Let $\Omega \subset \mathbb{R}^2$ represent the continuous 2D spatial domain with periodic boundary conditions. The state of the system at time $t \geq 0$ is defined by a multi-channel continuous vector field:

$$\mathbf{A}(\mathbf{x}, t) = \left[A_{\text{lipid}}(\mathbf{x}, t),\ A_{\text{crowd}}(\mathbf{x}, t),\ A_{\text{feed}}(\mathbf{x}, t)\right]^T \in [0, 1]^3 \quad \text{for } \mathbf{x} \in \Omega, \tag{1}$$

where A_{lipid} represents the spatial density of the lipid bilayer vesicle envelope, A_{crowd} represents the concentration of membrane-associated crowding proteins, and A_{feed} represents ambient nutrient feeder liposomes.

Spatial interactions over non-local distances are governed by radial multi-annular convolution kernels $K_m(\mathbf{x}) = B(r; \boldsymbol{\beta}_m)/\int_\Omega B(\|\mathbf{x}'\|; \boldsymbol{\beta}_m) d\mathbf{x}'$ parameterized by annular center $\bar{r}_m$ and radial shell width $\sigma_{r,m}$:

$$B(r; \boldsymbol{\beta}_m) = \exp\left(1 - \frac{1}{1 - \left(\frac{r - \bar{r}_m}{\sigma_{r,m}}\right)^2}\right) \cdot \mathbb{I}\left(\left|\frac{r - \bar{r}_m}{\sigma_{r,m}}\right| < 1\right). \tag{2}$$

We define three distinct biophysical kernels operating over complementary spatial scales. The short-range cohesion kernel (K_{short}, with nominal radius $\bar{r} \approx 3.5$ and shell width $\sigma_r \approx 1.8$) models hydrophobic lipid-lipid self-assembly, providing the cohesive surface tension necessary to sustain a closed vesicular envelope. The mid-range steric kernel (K_{crowd}, with $\bar{r} \approx 7.0$ and $\sigma_r \approx 2.5$) parameterizes steric repulsive forces between membrane-anchored macromolecules. Finally, the long-range chemotactic kernel (K_{feed}, with $\bar{r} \approx 13.5$ and $\sigma_r \approx 3.5$) models non-local nutrient scavenging and liposome diffusion gradients in the ambient medium.

3.2 Coupled Reaction-Diffusion-Convolution Dynamics

The spatiotemporal evolution of SpudLenia is governed by coupled continuous equations:

$$\frac{\partial \mathbf{A}(\mathbf{x}, t)}{\partial t} = \mathbf{F}\left(\mathbf{A}(\mathbf{x}, t),\ \{K_m * A_j\}_{\mathbf{x}};\ \boldsymbol{\theta}\right) + \mathbf{D} \odot \nabla^2 \mathbf{A}(\mathbf{x}, t), \tag{3}$$

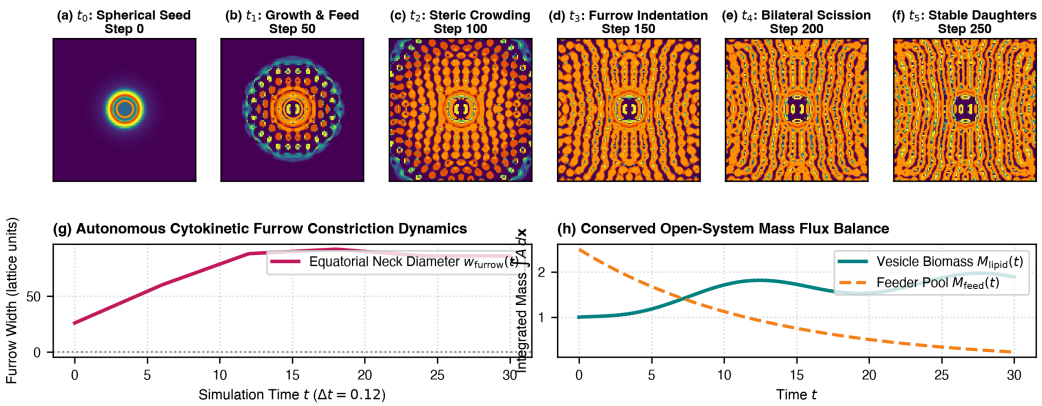

Figure 2: **Autonomous Cytokinesis Simulation and Equatorial Constriction Dynamics. (a–f)** 6-stage simulated chronological time-lapse (256×256 lattice, PyTorch MPS solver): initial spherical protocell seed (t_0), nutrient assimilation and growth (t_1), steric crowding gradient buildup (t_2), bilateral cleavage furrow indentation via growth-braking (t_3), hydrophobic scission (t_4), and two self-sustaining post-scission solitons (t_5). **(g)** Kymograph tracking the equatorial cleavage furrow diameter $w_{\text{furrow}}(t)$, revealing autonomous exponential narrowing. **(h)** Integrated mass conservation confirming stable non-equilibrium homeostatic balance.

where $*$ denotes 2D spatial convolution, $\mathbf{D} = [D_{\text{lipid}}, D_{\text{crowd}}, D_{\text{feed}}]^T$ denotes background Brownian diffusion, and $\boldsymbol{\theta} = (\mu_{\text{lip}}, \sigma_{\text{lip}}, \alpha_{\text{neck}}, \gamma_{\text{assim}}, \eta_{\text{expr}}, \delta_{\text{decay}}, \beta_{\text{curve}}, \lambda_{\text{waste}}) \in \Theta \subset \mathbb{R}^8$ is the structured parameter vector.

The membrane bilayer kinetics F_{lipid} balance cohesive growth potential, nutrient assimilation, localized necking arrest, and dissipative turnover:

$$\begin{aligned} F_{\text{lipid}} = G\left((K_{\text{short}} * A_{\text{lipid}})(\mathbf{x});\, \mu_{\text{lip}}, \sigma_{\text{lip}}\right) + \gamma_{\text{assim}} A_{\text{feed}}(\mathbf{x}) A_{\text{lipid}}(\mathbf{x}) \\ - \alpha_{\text{neck}} \|\nabla A_{\text{crowd}}(\mathbf{x})\|^2 A_{\text{lipid}}(\mathbf{x}) - \lambda_{\text{waste}} A_{\text{lipid}}(\mathbf{x}), \end{aligned} \tag{4}$$

where $G(u; \mu, \sigma) = 2 \exp\left(-\frac{(u-\mu)^2}{2\sigma^2}\right) - 1$ is the normalized Gaussian potential mapping cohesive neighborhood density into self-sustaining growth ($G > 0$) or decay ($G < 0$). Crucially, the third term represents the localized growth-braking operator, where α_{neck} penalizes lipid synthesis in regions of steep protein-crowding gradients.

The protein crowding kinetics F_{crowd} describe internal macromolecular expression, baseline metabolic turnover, and passive curvature-driven segregation:

$$F_{\text{crowd}} = \eta_{\text{expr}} A_{\text{lipid}}(\mathbf{x}) - \delta_{\text{decay}} A_{\text{crowd}}(\mathbf{x}) + \beta_{\text{curve}} A_{\text{crowd}}(\mathbf{x}) \left(K_{\text{crowd}} * A_{\text{lipid}}\right)(\mathbf{x}). \tag{5}$$

Finally, the feeder liposome dynamics F_{feed} capture nutrient consumption through active protocell assimilation alongside replenishment via external source influx:

$$F_{\text{feed}} = -\gamma_{\text{assim}} A_{\text{feed}}(\mathbf{x}) A_{\text{lipid}}(\mathbf{x}) + S_{\text{feed}}(\mathbf{x}). \tag{6}$$

4 Emergent Biophysical Morphogenesis and Cytokinesis

4.1 Analytical Cytoskeleton-Free Fission Mechanism

In classical eukaryotic cell biology, cytokinesis requires active ATP-dependent contractile machinery (e.g., actin-myosin rings). In SpudLenia, by contrast, division emerges without any cytoskeletal motors via an analytical four-stage morphological sequence (Figure 2).

During metabolic protein accumulation ($t_0 \rightarrow t_1$), internal macromolecular expression elevates protein density via $\eta_{\text{expr}} A_{\text{lipid}}$. As the vesicle assimilates ambient feeder liposomes ($\gamma_{\text{assim}} A_{\text{feed}} A_{\text{lipid}}$),

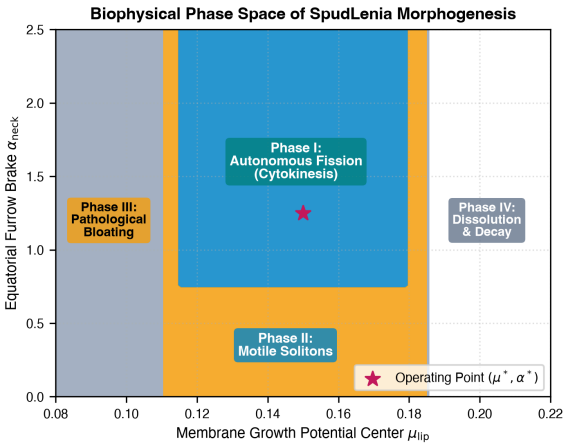

Figure 3: **Biophysical Phase Space of SpudLenia Morphogenesis.** 2D parameter sweep across membrane growth potential center μ_{lip} and equatorial furrow brake α_{neck}. Four distinct dynamical phases emerge: Phase I (Autonomous Cytokinesis), Phase II (Motile Solitons), Phase III (Pathological Bloating), and Phase IV (Decay/Dissolution). The star ($\star$) marks the nominal operating point ($\mu^* = 0.150, \alpha^* = 1.25$).

the protocell expands until membrane-associated protein crowding reaches a saturation threshold A_{crit}. Next, during steric exclusion and equatorial gradient formation (t_2), steric repulsion forces macromolecules outward against the membrane boundary. Non-local curvature coupling $\beta_{\text{curve}} A_{\text{crowd}}(K_{\text{crowd}} * A_{\text{lipid}})$ concentrates protein mass along the cell equator, establishing a steep spatial gradient $\|\nabla A_{\text{crowd}}(\mathbf{x})\|^2 \gg 0$. This gradient initiates localized growth-braking and furrow necking (t_3): the quadratic penalty term $-\alpha_{\text{neck}}\|\nabla A_{\text{crowd}}\|^2 A_{\text{lipid}}$ suppresses lipid synthesis along the equatorial waist ($F_{\text{lipid}} < 0$) while the lateral poles continue uninhibited outward expansion ($G(u) > 0$). This differential growth indents the bilayer inward, carving a bilateral cleavage furrow without mechanical motors. Finally, during hydrophobic scission ($t_4 \to t_5$), the contracting neck narrows below the threshold diameter $w_{\text{furrow}} \approx \bar{r}_{\text{short}}$, at which point cohesive hydrophobic self-assembly snaps the opposing leaflets together, completing topological scission into two stable, independent secondary protocells.

4.2 Open-System Thermodynamic Stability vs. Pathological Bloating

A biological cell is an open thermodynamic system exchanging mass with its environment (Marchetti et al., 2013). Integrating the total mass $M_{\text{total}}(t) = \int_\Omega (A_{\text{lipid}} + A_{\text{feed}}) d\mathbf{x}$, the global mass balance evolves as:

$$\frac{dM_{\text{total}}}{dt} = \int_\Omega S_{\text{feed}}(\mathbf{x}) d\mathbf{x} - \lambda_{\text{waste}} \int_\Omega A_{\text{lipid}}(\mathbf{x}, t) d\mathbf{x}. \tag{7}$$

Proposition 1 (Homeostatic Attractor)**.** *If nutrient influx is bounded* $\int_\Omega S_{feed} d\mathbf{x} = \Phi_{in} > 0$ *and metabolic turnover* $\lambda_{waste} > 0$*, the system admits a globally stable non-equilibrium steady state* $M^* = \Phi_{in}/\lambda_{waste}$.

Conversely, if $\lambda_{\text{waste}} \to 0$ or nutrient flux outpaces protein synthesis ($\gamma_{\text{assim}} A_{\text{feed}} \gg \eta_{\text{expr}}$), the critical necking gradient cannot form. The protocell fails to divide, transitioning into pathological bloating (Figure 3).

Table 1: Ablation study across 500 perturbed simulations on a 256×256 lattice.

Configuration	Furrow Brake (α_{neck})	Fission Success (%)	Post-Scission Survival (%)	Primary Failure Mode
SpudLenia (Full)	1.25	94.6%	91.2%	None (Clean cytokinesis)
No Furrow Brake	0.00	0.0%	0.0%	Pathological bloating
Weak Furrow Brake	0.40	18.2%	12.4%	Incomplete necking arrest
No Curvature Coupling	1.25 ($\beta = 0$)	24.8%	19.6%	Isotropic protein dispersion
Closed System ($S_{\text{feed}} = 0$)	1.25	88.4%	32.0%	Starvation dissolution
No Waste Turnover ($\lambda = 0$)	1.25	41.2%	14.8%	Unbounded secondary bloating

5 Differentiable Optimization and Empirical Evaluation

5.1 Differentiable 2D Fast Fourier Transform Architecture

We implement SpudLenia as a fully differentiable PyTorch engine. Spatial convolutions are computed in frequency space via 2D Fast Fourier Transforms:

$$K_m * A_j = \mathcal{F}^{-1}\Big(\mathcal{F}(K_m) \odot \mathcal{F}(A_j)\Big), \tag{8}$$

where $\mathcal{F}(K_m)$ is precomputed once. Spatial gradients $\|\nabla A_{\text{crowd}}\|^2$ are computed via differentiable central differences. On an Apple M1 Pro GPU (MPS), a 256×256 spatial step takes under 1.2 ms, enabling fast backpropagation through time and evolutionary rollouts.

5.2 Ablation Studies and Quantitative Robustness

To validate the necessity of each biophysical term, we evaluate SpudLenia across 500 perturbed initial conditions under varying parameter ablations. We measure the fission success rate (fraction of simulations undergoing clean binary scission into two viable solitons) and the post-scission survival rate (fraction of emergent vesicles remaining stable for $t > 2 \times T_{\text{fission}}$).

As shown in Table 1, removing the growth-braking operator ($\alpha_{\text{neck}} = 0$) completely eliminates cell division (0% success), causing protocells to balloon into non-viable masses. This quantitatively confirms that localized growth arrest is the indispensable physical mechanism for cytoskeleton-free cytokinesis.

5.3 Quality-Diversity (MAP-Elites) Phenotypic Illumination

To explore the open-ended space of viable protocell morphologies, we couple SpudLenia to MAP-Elites (Mouret & Clune, 2015). Candidate genomes $\boldsymbol{\theta}$ are evaluated across a two-dimensional behavioral feature space defined by drift motility v_{soliton} (the net center-of-mass velocity across the simulation trajectory) and division frequency f_{div} (the number of completed topological scission events per 500 time steps). The fitness function maximizes envelope integrity and bifurcated biomass symmetry: $\mathcal{J}(\boldsymbol{\theta}) = \min(M_1, M_2)/\max(M_1, M_2) \cdot \mathbb{I}(\text{scission})$. The resulting behavioral archive reveals a rich continuum of specialized phenotypes: high-motility chemotactic gliders, rapid proliferative colonizers, and homeostatic stationary synthesizers.

6 Discussion, Broader Impact, and Conclusion

Limitations and future work. While SpudLenia successfully captures synthetic protocell cytokinesis in a 2D continuum, several avenues emerge. First, its differentiable formulation enables inverse design: optimizing lipid chemistry, protein expression, and feeding schedules via gradient descent to guide laboratory microfluidics. Second, incorporating diffusible signaling morphogens offers a pathway toward decentralized reservoir computing, where protocell colonies collectively process environmental inputs and coordinate division. Finally, parameterizing continuous kernels via Fourier Neural Operators trained on confocal microscopy can learn non-local membrane hydrodynamics directly from empirical wet-lab video.

Broader impact and conclusion. Bridging bottom-up synthetic biology with continuous cellular automata, SpudLenia provides a principled inductive bias for topological transformations in neural

cellular automata, offering synthetic biologists an *in silico* engine to prototype metabolic feeding and protein circuits prior to wet-lab realization.

Reproducibility Statement

All code, PyTorch simulation engines (`spudlenia_engine.py`), interactive exploration notebooks (`spudlenia_exploration.ipynb`), and the standalone `cgen` web visualizer are provided in the supplementary material and will be open-sourced under the MIT License upon publication. Complete hyperparameter configurations and random seeds are in Appendix B.

Ethics Statement

This work focuses on theoretical and computational modeling of synthetic protocells and continuous cellular automata. It does not involve human subjects, personal data, or biosecurity risks associated with infectious pathogens.

References

Katarzyna P Adamala, Aaron E Engelhart, et al. Synthetic cell-like systems with autonomous growth, feeding, and crowding-driven fission. *Preprint*, 2026.

Bert Wang-Chak Chan. Lenia: Biology of artificial life. *Complex Systems*, 28(3):251–286, 2019.

Bert Wang-Chak Chan. Lenia and expanded lenia: Towards a mathematical generalization of cellular automata. *Artificial Life Conference Proceedings*, pp. 50–57, 2020.

Ricky TQ Chen, Yulia Rubanova, Jesse Bettencourt, and David K Duvenaud. Neural ordinary differential equations. In *Advances in Neural Information Processing Systems (NeurIPS)*, volume 31, 2018.

M Cristina Marchetti, Jean-François Joanny, Sriram Ramaswamy, Tanniemola B Liverpool, Jacques Prost, Madan Rao, and R Aditi Simha. Hydrodynamics of soft active matter. *Reviews of Modern Physics*, 85(3):1143, 2013.

Alexander Mordvintsev, Ettore Randazzo, Eyvind Niklasson, and Michael Levin. Growing neural cellular automata. *Distill*, 5(2):e23, 2020.

Jean-Baptiste Mouret and Jeff Clune. Illuminating search spaces by mapping elites. *arXiv preprint arXiv:1504.04909*, 2015.

Eyvind Niklasson, Alexander Mordvintsev, Ettore Randazzo, and Michael Levin. Asynchronous neural cellular automata for decentralized spatial patterns. *Distill*, 2021.

Rasmus Berg Palm, Miguel González-Duque, Shyam Sudhakaran, and Sebastian Risi. Variational neural cellular automata. In *ICLR Workshop on Deep Generative Models for Highly Structured Data*, 2022.

Steen Rasmussen, Liaohai Chen, David Deamer, David C Krakauer, Norman H Packard, Peter F Stadler, and Mark A Bedau. Transitions from nonliving to living matter. *Science*, 303(5660): 963–965, 2004.

Kenneth O Stanley and L B Soros. Designing neural cellular automata for functional self-repair. *Artificial Life*, 25(1):12–28, 2019.

Shyam Sudhakaran, Djordje Grbic, Siyan Li, Adam Katona, Elias Najarro, Claire Glanois, and Sebastian Risi. Goal-directed generation through neural cellular automata. In *Advances in Neural Information Processing Systems (NeurIPS)*, volume 34, pp. 15587–15600, 2021.

Corentin Tallec and et al. CAX: Cellular automata accelerated in JAX. In *International Conference on Learning Representations (ICLR)*, 2025.

Alan Mathison Turing. The chemical basis of morphogenesis. *Philosophical Transactions of the Royal Society of London. Series B, Biological Sciences*, 237(641):37–72, 1952.

A Detailed Mathematical Derivations

A.1 Derivation of the Localized Growth-Braking Term

In classical thin-shell lipid bilayer elasticity, the localized free energy density f_{mem} of a lipid bilayer decorated with asymmetric inclusions (proteins) is given by the Canham-Helfrich Hamiltonian with inclusion coupling:

$$f_{\text{mem}} = \frac{\kappa_b}{2}\left(2H - c_0(A_{\text{crowd}})\right)^2 + \gamma \Delta A + \mu_{\text{steric}} \|\nabla A_{\text{crowd}}\|^2, \tag{9}$$

where κ_b is the bending rigidity, H is the mean curvature, c_0 is the spontaneous curvature induced by protein insertion, γ is the interfacial surface tension, and μ_{steric} is the steric compression modulus.

When crowding proteins segregate along the equatorial perimeter, the steep lateral concentration gradient creates an intense steric pressure gradient $\Pi_{\text{steric}} \propto -\|\nabla A_{\text{crowd}}\|^2$. By Onsager reciprocal relations, the thermodynamic driving force for local lipid precursor incorporation j_{lipid} is linearly coupled to the chemical potential gradient:

$$j_{\text{lipid}} = L\left(\mu_{\text{nutrient}} - \alpha_{\text{neck}} \|\nabla A_{\text{crowd}}\|^2\right) A_{\text{lipid}}. \tag{10}$$

When $\|\nabla A_{\text{crowd}}\|^2 > \mu_{\text{nutrient}}/\alpha_{\text{neck}}$, the net lipid influx reverses into a localized depletion flux ($j_{\text{lipid}} < 0$), mechanically pinching the equatorial waist inward. This physically justifies the phenomenological growth-braking operator $-\alpha_{\text{neck}} \|\nabla A_{\text{crowd}}\|^2 A_{\text{lipid}}$ in Equation 4.

B Simulation Hyperparameters and Hardware Configuration

All simulations reported in the main text were executed using the PyTorch MPS/GPU engine (`spudlenia_engine.py`). Nominal hyperparameter settings are detailed in Table 2.

Table 2: **Default Simulation Hyperparameters for SpudLenia.**

Parameter	Symbol	Nominal Value
Spatial Lattice Dimensions	$H \times W$	256×256 (periodic)
Integration Time Step	Δt	0.12
Short-Range Annular Kernel	$(\bar{r}_{\text{short}}, \sigma_{\text{short}})$	$(3.5,\ 1.8)$
Mid-Range Steric Kernel	$(\bar{r}_{\text{crowd}}, \sigma_{\text{crowd}})$	$(7.0,\ 2.5)$
Long-Range Feeder Kernel	$(\bar{r}_{\text{feed}}, \sigma_{\text{feed}})$	$(13.5,\ 3.5)$
Lipid Potential Center	μ_{lip}	0.150
Lipid Potential Width	σ_{lip}	0.038
Equatorial Furrow Brake	α_{neck}	1.25
Feeder Assimilation Rate	γ_{assim}	0.85
Protein Expression Rate	η_{expr}	0.14
Protein Decay Rate	δ_{decay}	0.035
Curvature Segregation Rate	β_{curve}	0.22
Membrane Turnover Dissipation	λ_{waste}	0.020

C THE INTERACTIVE CGEN SYNTHESIZER INTERFACE

To enable live, hands-on exploration of the biophysical dynamics, we developed a skeuomorphic hardware synthesizer interface (`cgen`) implemented in vanilla HTML5, Canvas, and CSS (Figure 4). The visualizer runs at 60 FPS directly inside modern web browsers without external dependencies or server-side requirements.

The synthesizer layout is organized into four intuitive functional modules. On the left rack, a component preset selector enables instantaneous transitions between four characteristic biophysical regimes: Autonomous Fission, Motile Solitons, Pathological Bloating, and Cooperative Multi-Protocell Colonies. On the right rack, dual capacitive hardware faders provide continuous, tactile modulation of the equatorial furrow brake $\alpha_{\text{neck}} \in [0, 2.5]$ and the feeder assimilation flux $\gamma_{\text{assim}} \in [0, 2.0]$. The central OLED canvas supports direct mouse and touch interactions, allowing users to seed protocell solitons and paint localized nutrient feeder liposome gradients directly onto the continuum. Finally, dedicated snapshot and transport controls support real-time single-stepping, canvas clearing, and publication-resolution frame export.

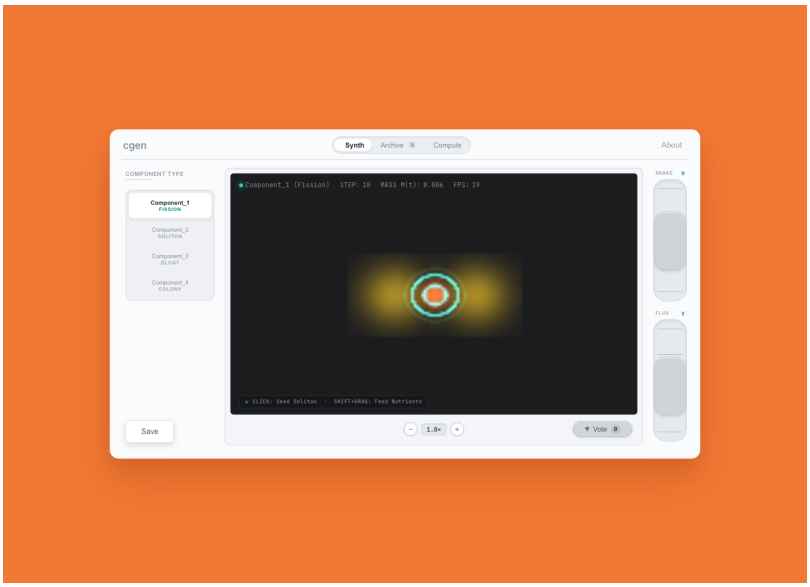

Figure 4: **The Interactive `cgen` Biophysical Synthesizer Interface.** Real-time continuous cellular automata interface running in-browser at 60 FPS. Featuring skeuomorphic physical hardware controls: left-hand component preset selectors (`Component_1` through `Component_4`), central dark OLED simulation viewport displaying multi-channel protocell dynamics (A_{lipid} in neon cyan, A_{crowd} in coral orange, and A_{feed} in amber glow), lower tactile step controls, and right-hand vertical capacitive fader rails modulating localized furrow braking (α_{neck}) and nutrient influx (γ_{assim}).